



Catalytic-site design for inverse heavy-enzyme isotope effects in human purine nucleoside phosphorylase

Rajesh K. Harijan^{a,1}, Ioanna Zoi^{b,1}, Dimitri Antoniou^b, Steven D. Schwartz^{b,2}, and Vern L. Schramm^{a,2}

^aDepartment of Biochemistry, Albert Einstein College of Medicine, Bronx, NY 10461; and ^bDepartment of Chemistry and Biochemistry, University of Arizona, Tucson, AZ 85721

Contributed by Vern L. Schramm, May 5, 2017 (sent for review March 23, 2017; reviewed by Jiali Gao and Nigel S. Scrutton)

Heavy-enzyme isotope effects (¹⁵N-, ¹³C-, and ²H-labeled protein) explore mass-dependent vibrational modes linked to catalysis. Transition path-sampling (TPS) calculations have predicted femto-second dynamic coupling at the catalytic site of human purine nucleoside phosphorylase (PNP). Coupling is observed in heavy PNPs, where slowed barrier crossing caused a normal heavy-enzyme isotope effect ($k_{\text{chem light}}/k_{\text{chem heavy}} > 1.0$). We used TPS to design mutant F159Y PNP, predicted to improve barrier crossing for heavy F159Y PNP, an attempt to generate a rare inverse heavy-enzyme isotope effect ($k_{\text{chem light}}/k_{\text{chem heavy}} < 1.0$). Steady-state kinetic comparison of light and heavy native PNPs to light and heavy F159Y PNPs revealed similar kinetic properties. Pre-steady-state chemistry was slowed 32-fold in F159Y PNP. Pre-steady-state chemistry compared heavy and light native and F159Y PNPs and found a normal heavy-enzyme isotope effect of 1.31 for native PNP and an inverse effect of 0.75 for F159Y PNP. Increased isotopic mass in F159Y PNP causes more efficient transition state formation. Independent validation of the inverse isotope effect for heavy F159Y PNP came from commitment to catalysis experiments. Most heavy enzymes demonstrate normal heavy-enzyme isotope effects, and F159Y PNP is a rare example of an inverse effect. Crystal structures and TPS dynamics of native and F159Y PNPs explore the catalytic-site geometry associated with these catalytic changes. Experimental validation of TPS predictions for barrier crossing establishes the connection of rapid protein dynamics and vibrational coupling to enzymatic transition state passage.

heavy enzyme | transition path sampling | purine nucleoside phosphorylase | enzyme design | femtosecond dynamics

Dynamic motions essential for enzyme catalysis occur on timescales from milliseconds for conformational changes to femtosecond bond vibrations associated with chemistry at catalytic sites. The millisecond motions are linked to structural changes during substrate binding (1) and product release, whereas the femtosecond motions are involved in transition state (TS) formation. Alterations of the femtosecond dynamics by isotope substitution in enzymes influence the probability of TS barrier crossing when protein femtosecond motions are coupled to chemistry at catalytic sites (2, 3).

The femtosecond dynamical effects in heavy purine nucleoside phosphorylase (PNP) on catalysis have been observed experimentally and have been explained by computational transition path sampling (TPS) (4, 5). TPS can provide insight into the atomic details of chemical reactions without prior knowledge of the reaction coordinate (6–8).

Human PNP is a homotrimer that catalyzes the reversible phosphorolysis of 6-oxypurine nucleosides and 6-oxypurine-2'-deoxynucleosides to generate the corresponding purine bases and α -D-ribose (or 2-deoxy- α -D-ribose) 1-phosphates (Fig. 1) (9). PNP provides the only metabolic pathway for the degradation of 2'-deoxyguanosine in human cells. Human genetic deficiency of PNP impairs expansion of activated T cells as a consequence of the accumulation of dGTP specifically in activated T cells. An unbalanced deoxynucleotide triphosphate pool leads to apoptotic cell death in the activated T-cell population, with no effect on quiescent

T cells (10). The inhibition of PNP is reported to be therapeutic in T-cell lymphoma and gout disease in clinical trials (11, 12).

The TS structure of human PNP has been solved by kinetic isotope effect (KIE) analysis and found to be a near fully dissociated ribocation, characteristic of a classic S_N1 mechanism (Fig. 1) (13). The purine leaving group and phosphate nucleophile are both activated by the enzyme, distorting the symmetry of the normal modes for phosphate and causing the bound purine to exhibit altered spectral properties (14, 15). In the femtosecond time period approaching the TS, His257 is hydrogen bonded to the ribosyl 5'-hydroxyl group and directs O5' toward the O4' of the purine ring, thus destabilizing the ribosidic bond to facilitate departure of the purine leaving group toward the TS (16). This motion of His257–O5'–O4' is one of the enzyme-reactant promoting vibrations, facilitating TS formation (4, 5). The motion is symmetrically coupled to the reaction coordinate and is distinct from the antisymmetrically coupled environmental bath that forms a Marcus theory-like environment (17).

The promoting vibrations of PNP, including His257 and its role in reaction chemistry, have been computationally studied by TPS (1). Heavy PNP labeled with ¹⁵N, ¹³C, and nonexchangeable ²H has slowed pre-steady-state catalytic-site chemistry and has a lower probability of barrier crossing, but unchanged steady-state kinetic properties (2). Slowed chemistry in heavy PNP has been interpreted as a mass-dependent slowed femtosecond dynamical search for the catalytic-site geometry permitting TS formation and barrier crossing. It has also been noted that heavy isotope-labeled

Significance

Protein design from first principles is developing rapidly for structural elements, binding domains, and protein-protein interactions. Design of structural elements to generate predictable changes in the fundamental properties of enzymatic catalysis remains challenging, requiring input from protein dynamics and the quantum chemical effects of transition state formation and barrier crossing. Human purine nucleoside phosphorylase (PNP) has a well-understood mechanism of catalysis, which includes rapid protein dynamics. PNP was used in a design program to alter the catalytic-site response to heavy-atom substitution in the enzyme protein. Native PNP exhibits slowed chemistry when made heavy with ²H, ¹³C, and ¹⁵N. We succeeded in designing a second-sphere mutation with improved promoting vibrations to catalyze faster chemistry in response to heavy PNP.

Author contributions: R.K.H. performed the experimental determinations; I.Z. and D.A. performed computational analysis and TPS calculations; S.D.S. and V.L.S. designed and supervised the project; R.K.H., I.Z., D.A., S.D.S., and V.L.S. analyzed the data; and R.K.H., I.Z., D.A., S.D.S., and V.L.S. wrote the paper.

Reviewers: J.G., University of Minnesota; and N.S.S., The University of Manchester.

The authors declare no conflict of interest.

¹R.K.H. and I.Z. contributed equally to this work.

²To whom correspondence may be addressed. Email: vern.schramm@einstein.yu.edu or ssschwartz@mail.arizona.edu.

This article contains supporting information online at www.pnas.org/lookup/suppl/doi:10.1073/pnas.1704786114/-DCSupplemental.

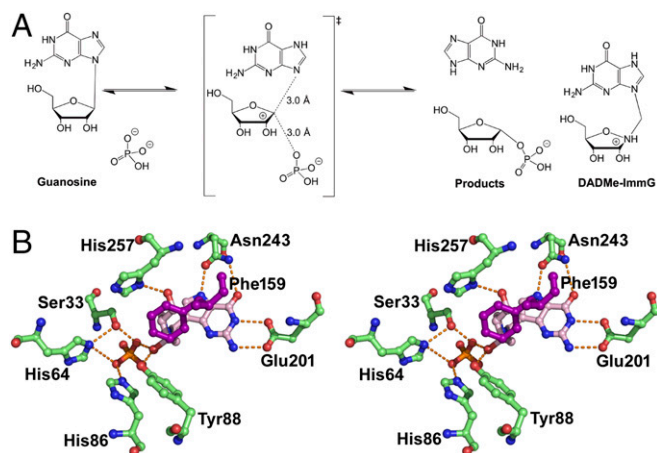


Fig. 1. (A) Guanosine phosphorolysis and TS of the reaction catalyzed by human PNP. The reaction is catalyzed in an S_N1 -like mechanism via a ribocationic TS. α -D-Ribose 1-phosphate and guanine are the products. DADMe-ImmG is a TS analog with a picomolar dissociation constant for human PNP. (B) Stereoview of the catalytic site of PNP-DADMe-ImmG- PO_4 crystal structure including residues Asn243, His257, and the position of Phe159, contributed from the neighboring monomer.

PNP alters the nuclear mass and bond vibrational frequencies without affecting the electrostatics of the enzyme according to the Born–Oppenheimer approximation (2). Speculation that heavy-enzyme effects in PNP are dominated by electronic properties of deuterium (18), rather than nuclear mass, has been disproven (3).

Here, we explored mutants of PNP by TPS analysis of amino acids adjacent to the residues directly involved in the catalytic site. The goal was to design a structural variant of heavy-enzyme PNP in which the heavy enzyme has an improved rate of catalytic-site chemistry by facilitating TS formation and barrier crossing. This design program was motivated by the combined TPS computational and experimental studies on native and heavy *Escherichia coli* dihydrofolate reductase. This enzyme differs from PNP by exhibiting no heavy-enzyme effect on barrier crossing (19, 20).

TPS calculations predicted that a F159Y mutation in PNP would facilitate barrier crossing in this altered heavy-atom PNP. Kinetic and structural characterization of light and heavy F159Y PNPs established that the TPS-predicted alterations in the femtosecond motions linked to chemical barrier crossing does indeed facilitate TS formation.

The $O5'-O4'$ atomic compression in native PNP is coordinated with TS barrier crossing, but in the native heavy enzyme, this motion is mistimed, leading to a less frequent formation of the TS (4). In addition, the value of this distance during the reaction event differs between the heavy and native PNP enzymes. In the heavy F159Y mutant, the heavy amino acids increase the probability of finding the TS, that is, the dynamical characteristics that lead to TS formation have been restored to overcome the heavy-atom effect. Specifically, both the timing of the compression and the extent of compression to its minimal value have been improved.

Results and Discussion

Enzyme Design Strategy. Our goal was to alter the catalytic effects that heavy isotopic substitution caused in the chemistry of human PNP relative to the light protein. After examination of the geometries of the active sites of the native and heavy enzymes and of the reactive trajectories of the previous analysis (5), the goal was to identify a residue close to His257 with an orientation that would favor either compression of the $His257-O5'-O4'$ oxygen atoms identified as the mass-influenced motion of His257, or directly influence the motion of $O5'$. The catalytic site of the PNP enzyme includes a residue, Phe159, belonging to the adjacent monomer, in

a hydrophobic loop, immediately coterminous to the ribosyl moiety (Fig. 1B). It is not a highly conserved amino acid among the PNPs. Its side chain is pointing toward the active site but is not in van der Waals contact with the reactants. The position of the aromatic ring is parallel to the His257 ring and is placed close to atoms ND1 of His257 and is therefore in a position to influence the motion of the $His257-O5'-O4'$ promoting vibration (Fig. 1B). The TPS analysis suggested that the orientation and location make Phe159 a candidate for mutation.

Mutation of Phe159 to tyrosine (hereafter F159Y) alters the character by adding a hydroxyl group. This mutation was selected with the expectation that the altered residue would help position His257 to interact favorably with $O5'$ in the heavy PNP and increase the probability of optimizing interactions toward the TS.

Effects of F159Y Mutation on Kinetics. Steady-state Michaelis–Menten kinetics for the light- and heavy-isotope-labeled PNPs were measured for guanosine phosphorolysis (Fig. S1). The k_{cat} and K_m values for light and heavy native PNPs, and for light and heavy F159Y PNPs are largely unchanged by enzyme mass. Purine leaving-group product release is rate limiting in steady-state kinetic analysis for human PNP and is limited by large loop motions (21). The kinetic results indicate the loop conformational changes related to product release are not strongly affected by mutating native PNP to F159Y PNP or by the mass change between the light and heavy F159Y PNPs (Fig. S2 and S3).

In contrast to the unchanged k_{cat} values found for heavy and light F159Y PNPs, the K_m value is modestly increased by the increased mass of F159Y PNP. Steady-state kinetic rates are governed by the slow conformational changes linked to substrate binding and product release. However, the enzymatic mass effects on the chemical step are also linked to the internal enzymatic step of barrier crossing, the probability of finding the TS for enzyme–substrate complexes. Guanosine bound to F159Y PNP shows a larger forward chemical commitment (see below), consistent with contributions from the chemical step in the K_m value according to the Michaelis–Menten formulation.

Catalytic-Site Chemistry Predicted by TPS. The dynamics of the $His257-O5'-O4'$ distance compression is altered by heavy-atom substitutions in native PNPs, and this $His257-O5'-O4'$ parameter is restored in the designed heavy F159Y PNP mutant (Table 1). Both light and heavy F159Y PNPs achieve full compression comparable to that of native light PNP. However, in the light F159Y, there is mistiming, as the $O5'-O4'$ distance compression is not coordinated with TS barrier crossing but happens well before the TS formation. Note in the heavy F159Y enzyme the compression is not mistimed. Note also that, in the native heavy enzyme, this compression was also mistimed, reaching its minimal value well after the TS has been formed.

Contour maps of the $O5'-O4'$ distance were developed as a function of reaction coordinate progression, measured by the

Table 1. PNP–guanosine- PO_4 $O5'-O4'$ distances in the reaction coordinate

PNPs	Minimum distance, Å	10 fs before From TS	At the TS, Å	At the TS, Å
Light PNP	2.53 ± 0.06	–17 to +3 fs	2.57 ± 0.04	2.56 ± 0.07
Heavy PNP	2.62 ± 0.10	+36 to +68 fs	2.93 ± 0.05	2.94 ± 0.06
Light F159Y PNP	2.56 ± 0.10	–40 to –15 fs	2.79 ± 0.08	3.02 ± 0.09
Heavy F159Y PNP	2.54 ± 0.06	–16 to –4 fs	2.59 ± 0.07	2.60 ± 0.06

The distances are the average of at least 120 barrier crossings from TPS analysis for each species of PNP.

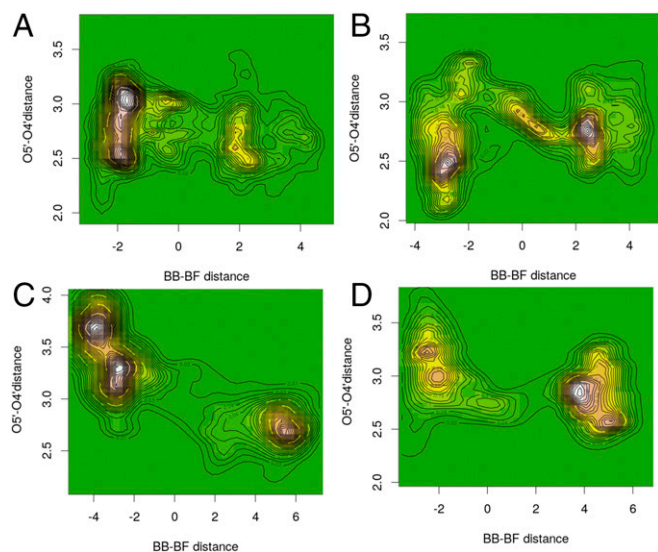


Fig. 2. Projections of histogrammed densities of the structures along all reaction trajectories on the plane of the O5'-O4' oxygen distance vs. bond-breaking (BB)-bond-forming (BF) distance, for native light PNP (A), native heavy PNP (B), light F159Y PNP (C), and heavy F159Y PNP (D). The "terrain" color map (green for "plains," i.e., zero density, up to white for "mountains," i.e., maximum density of structures) represents the allocation of a pair of the above distances among structures along the reaction path. Contour maps that join points with equal density have also been drawn.

difference of bond breaking at C1'-N9 minus the bond forming at C1'-O_p distances (Fig. 2). For the S_N1 mechanism of PNP, the TS is near zero on the abscissa (Fig. 2). Plots for all four enzymes, spanning the 500-fs TPS analysis, depict the probability for these specific measures derived from the ensembles of the 210 or 120 reactive trajectories generated with TPS for native and F159Y PNPs, respectively. They represent the most probable paths of reaction, when these paths are parameterized by the O5'-O4' and bond-breaking and bond-forming distances.

For native PNP, the O5'-O4' distance is highly populated at ~3 Å for the reactant state and becomes shorter as reactive trajectories approach the TS, where it reaches a minimum of 2.56 Å (Table 1 and Fig. 2A). Heavy F159Y reactive trajectories follow similar paths as the native enzyme, with the O5'-O4' reactant distance highly populated at 3.25 Å and reaching a minimum of 2.60 Å at the TS (Fig. 2D). In contrast, native heavy PNP reactive trajectories have the O5'-O4' distance highly populated at 2.5 Å for reactants (Fig. 2B). The distance increases along the reaction coordinate and has a distance of 2.94 Å at the TS. Finally, for the light F159Y PNP, the O5'-O4' distance is highly populated at 3.3-3.6 Å for reactants, and its distance decreases to only 3.02 Å at the TS, consistent with this being the least catalytically active species of these PNPs (Fig. 2C).

The difference in the dynamical behavior of His257-linked compression of the ribosyl O5'-O4' distance for heavy and light F159Y PNP is related to the probability of TS formation. This dynamic motion provides a partial explanation for the improved barrier crossing for heavy F159Y compared with the light F159Y.

Formation of the TS for PNP also requires purine leaving-group interactions to be coordinated with ribocation formation and phosphate activation. An additional leaving-group interaction is the double-hydrogen bond interaction between Asn243 and the purine base, and is considered below.

The geometrical properties of the TS structures for native and F159Y PNPs were examined to explore differences that can further illuminate the central differences (Table S1). The bond-breaking and bond-forming distances of the mutated enzymes at the TSs are different. Heavy F159Y and native PNPs are closely related, whereas the bond-breaking distance in light F159Y is larger by 0.5 Å and the bond-forming distance by 0.20 Å, a loose TS. Earlier studies with the TS structure of human PNP also demonstrated that mutations remote from the catalytic sites are capable of altering TS structure (22).

We also examined the differences of interaction between Asn243 and the purine leaving group for light and heavy F159Y PNPs (Fig. S4). The Asn243 interaction that corresponds to the TS (located near the zero of the abscissa) in the heavy F159Y is 2.82 Å. This close interaction does not occur in light F159Y PNP, where Asn243 is 3.8 Å away from the guanosine leaving group at the TS. Because this residue is important for stabilizing the leaving group, it plays a diminished role in light F159Y and is likely to contribute to the inverse heavy-atom isotope effect.

Experimental Analysis of Catalytic-Site Chemistry. The rate of the chemical step at the catalytic sites of light and heavy PNPs was determined for guanosine phosphorolysis by stopped-flow experiments in single-turnover conditions. The molar concentration of enzyme was in excess of the guanosine concentration to limit chemistry to a single catalytic event and thereby approximate first-order rate constants of guanine formation. This constant is independent of enzyme concentration, an essential experimental condition when comparing enzymes from different purifications. Guanosine in solution or bound to PNP is weakly fluorescent. Conversion to enzyme-bound guanine causes a fluorescent increase, which is lost when guanine is released to solution (15). The fluorescent signal of enzyme-bound guanine is thus a convenient measure of catalytic-site chemistry in PNP. Earlier studies of heavy-PNP catalysis used arsenolysis (2). Here, phosphorolysis was examined in both the computational TPS and the experimental determinations.

The F159Y mutation in PNP decreased the pre-steady-state chemistry (k_{chem}) 32-fold, from 263 to 8.3 per second. This decreased catalytic efficiency is seen only in single-turnover kinetics as the k_{cat} for steady-state kinetics is similar for native and F159Y PNPs. Similar steady-state kinetics is a consequence of slow product release as the rate-limiting step for PNPs (Table 2). The catalytic-site chemistry heavy-enzyme isotope effect ($k_{\text{chem, light}}/k_{\text{chem, heavy}}$) for native PNP was 1.31, with heavy enzyme slower compared with light enzyme, consistent with, and confirming earlier reports (2, 3). In contrast, the heavy-enzyme isotope effect ($k_{\text{chem, light}}/k_{\text{chem, heavy}}$) for heavy F159Y PNP was 0.75 with the chemical step increased in the heavy enzyme. The mutation has increased the probability of dynamic motions to find the TS configuration in heavy F159Y PNP relative to the light enzyme (Fig. 3 and Table 2). The absolute magnitude of the heavy-enzyme effect is similar, but opposite in sign, for the native and F159Y PNPs. This factor is the sum of timing and frequency influences of heavy-protein motions for the PNPs.

Table 2. Enzyme kinetic parameters of light and heavy PNPs

PNPs	k_{cat} , s ⁻¹	K_m , μM	k_{cat}/K_m , M ⁻¹ ·s ⁻¹	Forward commitment (Y)	Commitment factor (C _i)	k_{chem} , s ⁻¹	Heavy/light KIE
Light PNP	8.7 ± 0.2	34.1 ± 2.1	2.5 × 10 ⁵ ± 0.2	0.96 ± 0.01	24 ± 0.01	263 ± 9	1.31 ± 0.06
Heavy PNP	7.8 ± 0.3	39.9 ± 4.3	2.0 × 10 ⁵ ± 0.2	0.91 ± 0.02	10.1 ± 0.02	200 ± 6	
Light F159Y PNP	8.5 ± 0.3	56.4 ± 5.3	1.5 × 10 ⁵ ± 0.2	0.39 ± 0.003	0.64 ± 0.003	8.3 ± 0.4	0.75 ± 0.04
Heavy F159Y PNP	8.3 ± 0.4	54.2 ± 5.7	1.5 × 10 ⁵ ± 0.2	0.72 ± 0.01	2.6 ± 0.01	11.1 ± 0.2	

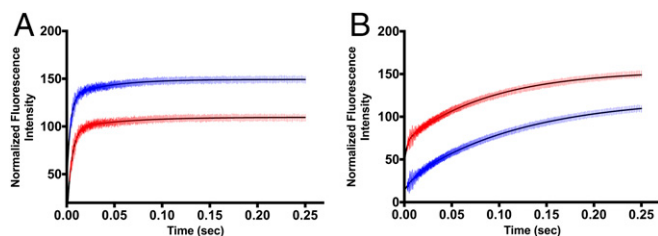


Fig. 3. Representative averaged stopped-flow traces for single-turnover experiments of wild-type (A) and F159Y PNP mutant (B) for guanosine phosphorolysis with 15 μ M PNP catalytic-site concentration and 5 μ M guanosine in 50 mM phosphate (*Materials and Methods*). Single turnovers were obtained. In A, the blue trace is light native PNP, and the red trace is heavy PNP. In B, the blue trace is light F159Y PNP, and the red trace is heavy F159Y PNP. The traces of A were fitted to a double-exponential fit, where the fast phase reports the catalytic-site chemistry rate (k_{chem}) followed by a slower conformational change affecting guanine fluorescence (15). The traces of B were fitted to a single exponential corresponding to the rate of guanine formation. The curves are offset for clarity. The catalytic-site enzyme chemistry rates of light and heavy PNPs are summarized in Table 2.

Dissociation Constant and Isotope Partition Analysis. PNP KIEs by stopped-flow analysis gives k_5 ($k_5 = k_{\text{chem}}$) from kinetic analysis (Fig. 3 and Mechanism 1). An independent analysis of the heavy-enzyme effects on catalysis can be obtained from the isotope partition experiments pioneered by Rose et al. (23). Isotope partition, also known as substrate-trapping or forward-commitment (C_f) experiments, follows the distribution of isotopically labeled guanosine (Fig. S5) from a PNP–guanosine complex after addition of excess unlabeled guanosine and phosphate to initiate the reaction or dissociation of bound, labeled guanosine (Mechanism 1). Pre-steady-state kinetic analysis indicates that the barrier for chemistry in native PNP is higher for heavy than light enzyme, but is lower for heavy than for light F159Y PNP (Fig. 3 and Table 2). For native PNP, guanosine isotope partition experiments demonstrated less bound guanosine converted to product in heavy than light enzyme (2). However, the inverse enzyme KIE for F159Y PNP predicts more bound guanosine should be converted to product in heavy than in light F159Y PNP complexes.

The fraction of bound guanosine converted to product (Y in Mechanism 1) is dependent on k_5 , the step forming ribose 1-phosphate (R1P) and on steps describing guanosine release without reaction. Quantitation of the E-Guo complex requires knowledge of K_d for heavy and light enzymes. We used the isotope partition method with varied guanosine concentrations to establish the K_d for guanosine under conditions of the isotope partition experiments (24, 25). The K_d values for light and heavy F159Y PNPs were 39 ± 8 and 42 ± 4 μ M, respectively (Fig. S6). These values agree well with the reported dissociation constant (K_d) of 40 μ M for the native PNP–guanosine complex (15).

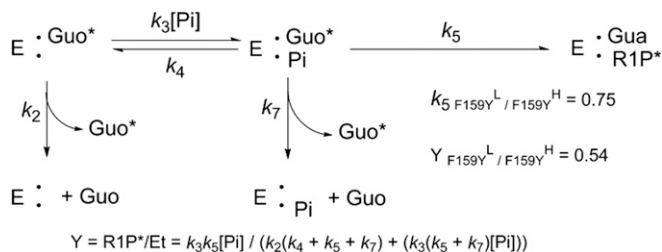
The forward-commitment factors (C_f) for light and heavy PNPs indicate the probability for reactants in the Michaelis complex to be converted to products relative to diffusive release to the solution reactant pool, expressed as the ratio of the rate constants for the chemical step to the rate constant of dissociation of the substrate from the enzyme–substrate complex ($C_f = k_{\text{chem}}/k_{\text{off}}$). The fractions of bound guanosine committed to guanosine phosphorolysis (Y in Mechanism 1) were 0.39 ± 0.003 and 0.72 ± 0.01 for light and heavy F159Y PNP, respectively (Fig. 4 and Table 2). The larger forward commitment of heavy F159Y PNP confirms the pre-steady-state analysis that the TS free-energy barrier for heavy F159Y PNP is lower than for light F159Y PNP, an independent analysis of the increased k_{chem} for heavy F159Y PNP. Values for Y obtained by isotope partition analysis also depend on denominator steps k_2 , k_4 , and k_7 . A small increase in one (or more) of these constants for heavy F159Y PNP readily accounts for the slightly larger than expected heavy-isotope Y value (Mechanism 1, and Table 2).

Opposite to the heavy F159Y PNP effect, catalytic-site guanosine phosphorolysis for native light and heavy PNP gave 0.96 ± 0.01 and 0.91 ± 0.02 fractional trapping of bound guanosine, respectively, consistent with a lower TS barrier for the light form of native PNP (Fig. 4 and Table 2).

Structure of F159Y PNP in Complex with DADMe–ImmG. The crystal structure of F159Y PNP in complex with DADMe–ImmG (a TS analog) and phosphate was determined at 2.2 \AA using crystals obtained by cocrystallizations (detailed in *Materials and Methods*). The crystal structures of native unliganded [Protein Data Bank (PDB) ID code 1M73] and DADMe–ImmG-bound PNP (PDB ID code 3PHB) are known (26, 27). The structure of the F159Y PNP–DADMe–ImmG– PO_4 complex was solved in the $P2_12_12_1$ space group with two F159Y PNP trimers in the asymmetric unit (Table S2). The density of DADMe–ImmG is clearly defined in the structure (Fig. 5). Except for the N-terminal His₆ tag, all backbone amino acids were readily fit into the electron density map. A solvent-exposed loop (residues 59–63) with high B factors produced weak density for its side-chain residues.

DADMe–ImmG is bound in the active site with low B factors, similar to the surrounding protein (Fig. 5). The O3' of DADMe–ImmG is hydrogen bonded to the hydroxyl of (Tyr88), whereas the O5' is hydrogen bonded to the side-chain N of His257 (ND1). The His257 in F159Y is offset slightly from its position in native PNP, moved slightly away from bound DADMe–ImmG (Fig. 5). However, the hydrogen bond distance to the O5' is 2.7, compared with 2.8 \AA in native PNP, within error of the experimental analysis, indicating that the bound DADMe–ImmG maintains a similar hydrogen bond interaction. Tyrosine in the F159Y variant was found to hydrogen bond with the hydroxyl group of the adjacent Tyr88. Tyr159 does not make direct contact with catalytic-site reactants. Its nearest approach is to the O3' of DADMe–ImmG at 3.9 \AA (Fig. 5). The F159Y substitution thus moves His257 and Y159 both slightly away from catalytic-site reactants relative to the native PNP–DADMe–ImmG– PO_4 complex, consistent with its lower k_{chem} . No other structural changes are apparent near the catalytic site of F159Y PNP (Fig. 5 and Fig. S7). The binding contacts of DADMe–ImmG are the same in native (PDB ID code 3PHB) and F159Y PNP (PDB ID code 5UGF; Fig. S7), within structural uncertainty.

Comparison of TPS and Crystallographic PNP Structures. TPS analysis generated reactant-path structures at the TS for heavy and light native and F159Y mutant PNPs. These can be compared with the crystal structures of PNP with DADMe–ImmG and PO_4 , which is related to the TS by the TS analog interaction. From TPS analysis, no significant differences are evident in the orientation of His257



Mechanism 1. Guanosine isotope partition experiment for F159Y PNP. [$1\text{-}^{14}\text{C}$]Guanosine (Guo*) bound to F159Y PNP partitions to product $\alpha\text{-D-}[1\text{-}^{14}\text{C}]$ ribose 1-phosphate (R1P) by k_5 or is released unchanged by steps $k_2 + k_4 + k_7$ when mixed with excess unlabeled guanosine (Guo) and inorganic phosphate (Pi). The fraction of bound Guo* converted to product (Y) is given by the equation (25). The values for k_5 are obtained independently from pre-steady-state kinetics (Fig. 3B). The value for Y is obtained from the isotope partition experiment.

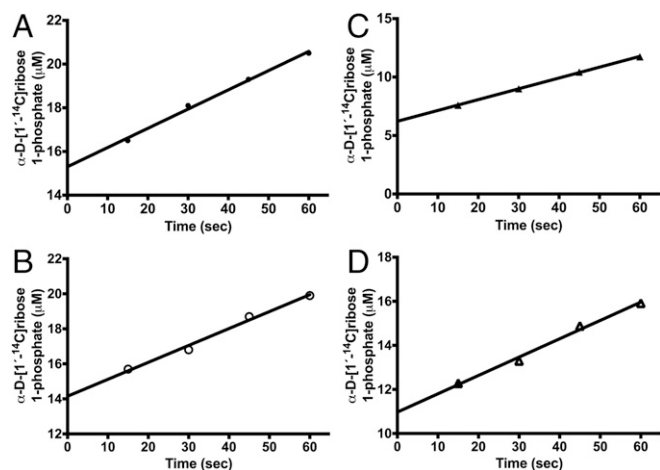


Fig. 4. Experimental data of $[1\text{-}^{14}\text{C}]$ guanosine trapping in the Michaelis complex of PNPs. The ordinate shows the amount of bound reactant committed to product formation in the phosphorolysis of guanosine by PNPs. Equilibrated mixtures of $25\ \mu\text{M}$ PNPs and $80\ \mu\text{M}$ $[1\text{-}^{14}\text{C}]$ guanosine (Fig. S5) were mixed with excess guanosine and phosphate at time = 0. The amount of $[1\text{-}^{14}\text{C}]$ guanosine converted to $[1\text{-}^{14}\text{C}]\alpha\text{-D-ribose 1-phosphate}$ was extrapolated to $t = 0$ and compared with the initial PNP- $[1\text{-}^{14}\text{C}]$ guanosine concentration to calculate Y of Table 2. Guanosine commitment for light and heavy native PNP are shown in A and B, respectively. Guanosine commitment for light and heavy F159Y PNP are shown in C and D, respectively. The values of Y and C_f are summarized in Table 2.

in the F159Y mutant at or near the TS with all His257ND1 – O5' distances near $2.8\ \text{\AA}$. There is a significant change in the interaction of Tyr88, found in a hydrogen bond to O3' of DADMe-ImmG in crystal structures. At the TS for F159Y PNP, TPS indicates this distance to be 3.4 and $2.9\ \text{\AA}$ in the light and heavy F159Y PNPs, respectively. Here, the interaction in the heavy enzyme favors TS formation (Table S3 and Fig. S8). A significant difference appears in the weak interaction between guanosine and Asn243 ($3.8\ \text{\AA}$ at the TPS TS; see above) in F159Y PNP, whereas this is a favorable interaction of $2.9\ \text{\AA}$ in the crystal structure and is unchanged from native and F159Y PNPs. This difference at the TS is accessible only through the TPS computational approach.

Further analysis of TPS trajectories at the atomistic level reveals differences for the orientations and relative positions of His257 and Phe159 (mutated to Tyr159) at the TS. As shown in Table S4 and Fig. S9, the distance between CE2 of the 159 residue and ND1 of residue His257 is $3.95\ \text{\AA}$ for the native light and $3.85\ \text{\AA}$ for the light mutant. The difference between native/mutant light for the distance between CZ of residue 159 and ND1 of His257 is $0.5\ \text{\AA}$. The orientation of these two residues is almost identical, taking as

reference the angle formed by atom CE2 of residue 159 and atoms CG and NE2 of His257. However, in the light mutant, the tyrosine ring has shifted, so that the oxygen atom of the tyrosine ring faces the nitrogen atom (ND1) of the histidine.

For the native heavy and heavy mutant, the orientation of His257 and Phe159 (mutated to Tyr159) does not change significantly, but some important distances do change: the distance between CE2 of the residue 159 and ND1 of residue 257 for the native heavy is $3.97\ \text{\AA}$, whereas for the heavy mutant it is $4.59\ \text{\AA}$. Similarly to the light enzymes, we note that the tyrosine ring is slightly shifted and tilted, and in a direction perpendicular to the histidine ring the tyrosine oxygen lies directly above the ND1 atom of the histidine ring, which explains the difference in the distances mentioned above.

In summary, the dynamical characteristics that lead to the TS are different between heavy F159Y and light PNP. Specifically, in light F159Y, the O5'–O4' compression is mistimed, the enzyme exhibits a loose TS, and the interaction of Asn243 that stabilizes the leaving group is weak and plays a diminished role. In addition, we observed a change in the interactions between Tyr88 and the ribose moiety, which are stronger for the heavy F159Y and favor TS formation, and saw differences in the relative position and orientation between Tyr159 and His257. All of the above contribute to the inverse heavy-enzyme isotope effect.

Concluding Remarks. Complex motions of amino acids and reactants at the catalytic site of PNP vary on the femtosecond timescale to alter the electrostatic forces forming the TS. In heavy PNP, increased mass alters this dynamical search for the TS, leading to a decrease in the probability of barrier crossing. Our goal here was to use TPS to design a simply modified PNP with altered catalytic-site dynamics to increase the probability of finding the TS in an isotopically heavy enzyme. As no such enzymes have yet been reported, there are computational and experimental challenges to this goal. TPS analysis suggested the F159Y mutation would increase the probability of TS formation in a heavy enzyme by restoring important femtosecond motions linked to barrier crossing. The computational design was tested experimentally and fully supported this prediction.

Materials and Methods

Computational Methods. We used transition path sampling (6–8) to generate and analyze reactive trajectories and the TS ensemble. TPS is a Monte Carlo search in reactive trajectory space where trajectories are generated according to a Boltzmann distribution; therefore, their ensemble represents the most dynamically probable reactive pathways. We used the CHARMM (28) molecular dynamics package for all simulations. We generated 210 and 120 reactive trajectories of 500 fs for the native and mutated PNPs, respectively. From the harvested reactive trajectories, we identified a TS ensemble of 25 uncorrelated TS structures for the native enzymes and 20 for the mutated enzyme. The contour maps in Fig. 2 were calculated with the R statistics package. Full computational details are available in Supporting Information.

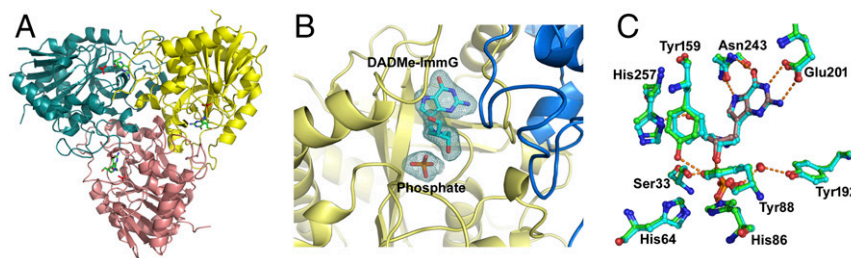


Fig. 5. The crystal structure and subunit-subunit interaction of PNP in complex with DADMe-ImmG and inorganic phosphate. (A) The crystal structure of trimeric human PNP. (B) The omit ($F_o - F_c$) difference electron density map of the DADMe-ImmG structure at 3.0σ contour level. The ($F_o - F_c$) difference maps were calculated after 15 cycles of omit refinement by REFMAC5, leaving out the subunit B active-site DADMe-ImmG ligand. The DADMe-ImmG of subunit B (yellow color), bound at the active site, is also surrounded by subunit C (blue color). (C) Superposition of active site residues of wild type (cyan; PDB ID code 3PHB) and F159Y PNP (green; PDB ID code 5UGF) PNPs bound to the TS-analog DADMe-ImmG. New hydrogen bonds appearing as a consequence of the F159Y substitution are shown as dashed lines to Tyr159 and Tyr88. A stereoview version of C is shown in Fig. S7.

Site-Directed Mutagenesis. Site-directed mutagenesis to introduce the second-sphere mutation F159Y in PNP used the Q5 site-directed mutagenesis kit from New England Biolabs as outlined in [Supporting Information](#).

Expression and Purification of Light and Heavy PNPs. The natural abundance (light) and heavy PNPs (wild type and F159Y mutant) were expressed in *E. coli* (DE3)pLysS strain using a pCR-T7/NT-TOPO expression vector. The expressed PNPs contained 6-histidine affinity tag at the N terminus. The purification of light and heavy PNPs were done as described previously with some modifications, as described in [Supporting Information](#) (5).

Steady-State Kinetics. The enzyme kinetics of light and heavy PNPs were performed using a Cary-100 spectrophotometer (Varian) at 25 °C. Reaction mixtures contained 50 mM Tris-HCl (pH 7.4), 50 mM inorganic phosphate (Pi), pH 7.4, and varying guanosine concentrations (10–160 μM). Absorbance was recorded at 258 nm after addition of 10 nM light- or heavy-PNP enzymes. The initial rates of absorbance change were calculated with the Varian software. The molar extinction coefficient of $-5,500 \text{ M}^{-1}\text{cm}^{-1}$ was used for the conversion of guanosine to guanine. The kinetic data fitting was done using Eq. 1, where ν is the initial velocity, V is the maximal velocity, S is the concentration of variable substrate, and K_m is the Michaelis constant for the variable substrate:

$$\nu = (V \times [S]) / ([S] + K_m). \quad [1]$$

Single-Turnover Rate Constant. Single-turnover pre-steady-state constants were determined using stopped-flow spectrofluorometer (Applied Photophysics; dead time, ≤ 1.25 ms) at 25 °C. The increase in the fluorescence signal was measured upon the formation of enzyme-bound guanine. The reaction was excited at 280 nm with slit width of 1 mm, and the fluorescence signal above

305 nm was collected using WG305 Scott filter positioned between the photomultiplier and the sample cell. The fluorescence spectra were monitored for 250 ms, and 1,000 points were collected for individual rate curve analysis. Syringe-1 contained 50 mM Tris-HCl (pH 7.4), 50 mM Pi (pH 7.5), and 30 μM either light- or heavy-PNP enzymes. Syringe-2 contained 50 mM Tris-HCl (pH 7.5), 50 mM Pi (pH 7.4), and 10 μM guanosine.

Dissociation Constant and Commitments of F159Y PNP–Guanosine Complex. The dissociation constants (K_d) and forward-commitment factors (C_f) of light and heavy F159Y PNP–guanosine complexes were determined using isotope-trapping methods of Rose et al. (23, 24), as detailed in [Supporting Information](#).

Cocrystallization, Structure Determination, Refinement, and Analysis. Light F159Y PNP and DADMe–Immucillin-G (DADMe–ImmG) were used for the crystallographic inhibitor binding studies as detailed in [Supporting Information](#).

ACKNOWLEDGMENTS. We acknowledge Drs. Scott Cameron and Hilda Namanja-Magliano for insightful discussions and suggestions. The use of the facilities and expertise of the Albert Einstein College of Medicine crystallization, data collection, and proteomics core facility is gratefully acknowledged. The intensity datasets used for the refined structures were collected at Lilly Research Laboratories Collaborative Access Team Advanced Photon Source beamline, which is gratefully acknowledged. All computer simulations were performed at the University of Arizona High-Performance Computing Center on an SGI Altix ICE 8400 supercomputer. This research was supported through NIH Program Project Grant GM068036 (to V.L.S. and S.D.S.).

- Núñez S, Wing C, Antoniou D, Schramm VL, Schwartz SD (2006) Insight into catalytically relevant correlated motions in human purine nucleoside phosphorylase. *J Phys Chem A* 110:463–472.
- Silva RG, Murkin AS, Schramm VL (2011) Femtosecond dynamics coupled to chemical barrier crossing in a Born-Oppenheimer enzyme. *Proc Natl Acad Sci USA* 108:18661–18665.
- Suarez J, Schramm VL (2015) Isotope-specific and amino acid-specific heavy atom substitutions alter barrier crossing in human purine nucleoside phosphorylase. *Proc Natl Acad Sci USA* 112:11247–11251.
- Antoniou D, Ge X, Schramm VL, Schwartz SD (2012) Mass modulation of protein dynamics associated with barrier crossing in purine nucleoside phosphorylase. *J Phys Chem Lett* 3:3538–3544.
- Zoi I, et al. (2016) Modulating enzyme catalysis through mutations designed to alter rapid protein dynamics. *J Am Chem Soc* 138:3403–3409.
- Antoniou D, Schwartz SD (1998) Proton transfer in benzoic acid crystals: Another look using quantum operator theory. *J Chem Phys* 109:5487–5493.
- Bolhuis P, Dellago C (2015) Practical and conceptual path sampling issues. *Eur Phys J Spec Top* 224:2409–2427.
- Dellago C, Bolhuis P (2007) Transition path sampling simulations of biological systems. *Top Curr Chem* 268:291–317.
- Giblett ER, Ammann AJ, Wara DW, Sandman R, Diamond LK (1975) Nucleoside-phosphorylase deficiency in a child with severely defective T-cell immunity and normal B-cell immunity. *Lancet* 1:1010–1013.
- Nyhan WL (2005) Disorders of purine and pyrimidine metabolism. *Mol Genet Metab* 86:25–33.
- Dummer R, et al. (2014) Final results of a multicenter phase II study of the purine nucleoside phosphorylase (PNP) inhibitor forodesine in patients with advanced cutaneous T-cell lymphomas (CTCL) (mycosis fungoides and Sézary syndrome). *Ann Oncol* 25:1807–1812.
- Sattui SE, Gaffo AL (2016) Treatment of hyperuricemia in gout: Current therapeutic options, latest developments and clinical implications. *Ther Adv Musculoskelet Dis* 8:145–159.
- Lewandowicz A, Schramm VL (2004) Transition state analysis for human and *Plasmodium falciparum* purine nucleoside phosphorylases. *Biochemistry* 43:1458–1468.
- Deng H, Lewandowicz A, Schramm VL, Callender R (2004) Activating the phosphate nucleophile at the catalytic site of purine nucleoside phosphorylase: A vibrational spectroscopic study. *J Am Chem Soc* 126:9516–9517.
- Ghanem M, et al. (2008) Tryptophan-free human PNP reveals catalytic site interactions. *Biochemistry* 47:3202–3215.
- Núñez S, Antoniou D, Schramm VL, Schwartz SD (2004) Promoting vibrations in human purine nucleoside phosphorylase. A molecular dynamics and hybrid quantum mechanical/molecular mechanical study. *J Am Chem Soc* 126:15720–15729.
- Schwartz SD (1996) Quantum activated rates—an evolution operator approach. *J Chem Phys* 105:6871–6879.
- Kohen A (2015) Role of dynamics in enzyme catalysis: Substantial versus semantic controversies. *Acc Chem Res* 48:466–473.
- Dametto M, Antoniou D, Schwartz SD (2012) Barrier crossing in dihydrofolate reductase does not involve a rate-promoting vibration. *Mol Phys* 110:531–536.
- Wang Z, Antoniou D, Schwartz SD, Schramm VL (2016) Hydride transfer in DHFR by transition path sampling, kinetic isotope effects, and heavy enzyme studies. *Biochemistry* 55:157–166.
- Ghanem M, Zhadin N, Callender R, Schramm VL (2009) Loop-tryptophan human purine nucleoside phosphorylase reveals submillisecond protein dynamics. *Biochemistry* 48:3658–3668.
- Luo M, Li L, Schramm VL (2008) Remote mutations alter transition-state structure of human purine nucleoside phosphorylase. *Biochemistry* 47:2565–2576.
- Rose IA, O'Connell EL, Litwin S (1974) Determination of the rate of hexokinase-glucose dissociation by the isotope-trapping method. *J Biol Chem* 249:5163–5168.
- Rose IA (1980) The isotope trapping method: Desorption rates of productive E.S complexes. *Methods Enzymol* 64:47–59.
- Cleland WW (1975) Partition analysis and the concept of net rate constants as tools in enzyme kinetics. *Biochemistry* 14:3220–3224.
- Ealick SE, et al. (1990) Three-dimensional structure of human erythrocytic purine nucleoside phosphorylase at 3.2 Å resolution. *J Biol Chem* 265:1812–1820.
- Ho MC, et al. (2010) Four generations of transition-state analogues for human purine nucleoside phosphorylase. *Proc Natl Acad Sci USA* 107:4805–4812.
- Brooks BR, et al. (2009) CHARMM: The biomolecular simulation program. *J Comput Chem* 30:1545–1614.
- Parkin DW, Leung HB, Schramm VL (1984) Synthesis of nucleotides with specific radiolabels in ribose. Primary ^{14}C and secondary ^3H kinetic isotope effects on acid-catalyzed glycosidic bond hydrolysis of AMP, dAMP, and inosine. *J Biol Chem* 259:9411–9417.
- Silva RG, Hirschi JS, Ghanem M, Murkin AS, Schramm VL (2011) Arsenate and phosphate as nucleophiles at the transition states of human purine nucleoside phosphorylase. *Biochemistry* 50:2701–2709.
- Schramm VL (1999) Enzymatic transition-state analysis and transition-state analogs. *Methods Enzymol* 308:301–355.
- Winn MD, et al. (2011) Overview of the CCP4 suite and current developments. *Acta Crystallogr D Biol Crystallogr* 67:235–242.
- Adams PD, et al. (2010) PHENIX: A comprehensive Python-based system for macromolecular structure solution. *Acta Crystallogr D Biol Crystallogr* 66:213–221.
- McCoy AJ, et al. (2007) Phaser crystallographic software. *J Appl Cryst* 40:658–674.
- Emsley P, Cowtan K (2004) Coot: Model-building tools for molecular graphics. *Acta Crystallogr D Biol Crystallogr* 60:2126–2132.
- Murshudov GN, Vagin AA, Dodson EJ (1997) Refinement of macromolecular structures by the maximum-likelihood method. *Acta Crystallogr D Biol Crystallogr* 53:240–255.
- Chen VB, et al. (2010) MolProbity: All-atom structure validation for macromolecular crystallography. *Acta Crystallogr D Biol Crystallogr* 66:12–21.